MATERIALS CHEMISTRY
FRONTIERS

CCS 中国化学会 CHINESE CHEMICAL SOCIETY
ICCAS
ROYAL SOCIETY OF CHEMISTRY

RESEARCH ARTICLE

View Article Online
View Journal | View Issue

Cite this: *Mater. Chem. Front.*, 2025, **9**, 2646

NiO nanowires in nanofluids based on a PDMS-type fluid†

Desireé De los Santos, * Juan Jesús Gallardo, Iván Carrillo-Berdugo, María Gragera-García, Saray Gragera-García, Violeta Guillén, R. Alcántara and Javier Navas *

Improving the efficiency of environmentally friendly energy sources such as solar energy is one of the basic objectives for developing the ecological transition required by our society. Thus, in this work, nanofluids based on NiO nanowires and a polydimethylsiloxane (PDMS) fluid are developed to improve the efficiency of parabolic trough-based concentrating solar power plants (CSP-PTC). To this end, NiO nanowires are successfully synthesized in our laboratory and used to prepare nanofluids. Their physical stability is thoroughly characterized. Subsequently, the properties of interest for the application of these nanofluids as heat transfer fluids are characterized. These properties were surface tension, density, dynamic viscosity, isobaric specific heat and thermal conductivity. Based on these properties, the efficiency improvement of CSP-PTC systems is estimated, achieving improvements of up to 5% with the designed nanofluids.

Received 2nd April 2025,
Accepted 14th July 2025

DOI: 10.1039/d5qm00283d

rsc.li/frontiers-materials

1. Introduction

One of the main goals in society today is the production of energy from environmentally-friendly sources that do not contribute to climate change. To this end, improving the overall efficiency of renewable energy sources is crucial, with solar energy being one of the most significant. Within the realm of solar energy, recent studies have accelerated the development of concentrated solar power (CSP), which generates electricity using the sun's energy. This technology focuses solar energy onto a heat transfer fluid capable of storing and transporting heat to produce steam that drives a turbine, generating electricity. Among the different CSP technologies, parabolic trough collectors (CSP-PTC) are among the most widely used. In this technology, heliostats with a parabolic trough shape focus solar radiation onto an absorber tube. A synthetic oil circulates through the tube, operating at temperatures of up to approximately 673 K. This fluid reaches a heat exchanger, producing steam to move the turbine. The efficiency of the collectors and heat exchanger depends heavily on the thermophysical and rheological properties of this synthetic oil, so improving its properties can enhance the overall efficiency of CSP-PTC plants.

One strategy that has attracted attention in recent years to improve heat transfer efficiency is the use of nanofluids, colloidal suspensions of nanomaterials. Nanofluids often exhibit superior thermal properties to the base fluid, making them promising for heat transfer applications. Recent research has investigated nanofluids based on several fluids and nanomaterials in great depth.[1]

The long-term stability of these nanofluids is crucial to enhance these thermal properties. Factors such as the base fluid, nanoparticle properties, the surfactant and synthesis method play a critical role in achieving this stability. The choice of the base fluid for nanofluid preparation is typically determined by the operating temperature of the heat transfer process. In the case of CSP-PTC plants, where temperatures reach around 673 K, synthetic oils are commonly used. The most widespread fluid in these plants, a eutectic mixture of biphenyl and diphenyl oxide, poses issues due to its toxicity, irritability, and environmental impact. Polydimethylsiloxane (PDMS) fluids represent an alternative with comparable thermal properties, reduced toxicity and enhanced operational safety.[2] These fluids, known as linear silicone fluids due to their structure as linear polymers of dimethyl siloxane, require their thermal properties to be enhanced before being suitable for CSP-PTC applications, particularly thermal conductivity and heat capacity.

Metal oxide nanofluids are promising for enhancing the efficiency of CSP-PTC plants. Studies have demonstrated improvements in thermal properties including thermal conductivity and specific heat capacity when incorporating nanoparticles such as NiO, ZnO, CuO, SiO_2, MgO, and Fe_3O_4 into heat transfer fluids.[3] These enhancements are attributed to

Department of Physical Chemistry, University of Cádiz, E-11510 Puerto Real, Spain. E-mail: desire.delossantos@uca.es, javier.navas@uca.es

† Electronic supplementary information (ESI) available. See DOI: https://doi.org/10.1039/d5qm00283d

mechanisms like Brownian motion and interfacial thermal resistance.[4] Simulations predict significant increases in overall CSP-PTC system performance, with efficiency improvements of up to 34.8% for surface collectors and 34.3% for volumetric collectors using NiO nanowire dispersed in the conventional fluid used, the eutectic mixture of biphenyl and diphenyl oxide.[5] In addition, using the same fluid and Fe_3O_4 nanoparticles, promising results were found, with a 9% improvement in thermal conductivity and increased plant efficiency.[3b] However, the suitability of nanofluids for volumetric absorption in parabolic-trough collectors requires careful consideration of their optical, rheological, and thermal properties.[6] Nanofluids offer enhanced thermophysical properties but face stability challenges and achieving stable nanofluids is crucial for high-temperature applications.[7] In this context, the use of surfactants could constitute an effective strategy to increase their colloidal stability.[8] However, the optimal surfactant type and concentration may vary depending on the specific nanofluid composition and intended application.[9] It is imperative to carefully evaluate the advantages and disadvantages of this approach, considering the particularities of each system and the intended applications. The selection of the surfactant will depend on the properties of the nanoparticles, the dispersion medium, and the compatibility with the other components of the nanofluid to prevent unwanted interactions.

This work analyses the stability and thermal efficiency of NiO/PDMS nanofluids with NiO nanowires synthesized in our laboratory used as the nanomaterial. The surfactant used has the trade name SPAN20, and the physical stability of the colloidal suspension with and without surfactant was evaluated. Thermal efficiency was analysed by means of measurements of the following key properties; density, surface tension, viscosity, heat capacity and thermal conductivity.

2. Experimental

2.1. Synthesis of NiO nanowires

NiO nanowires (NiO_{NW}) were synthesized using the hydrothermal method described by Dang *et al.*[10] First, 3.65 mmol of nickel(II) chloride ($NiCl_2$, purity $\geq$ 99.9%, Sigma-Aldrich) was dissolved in a 1 : 2 mixture of deionized water and ethylene glycol (purity $\leq$ 99.50%, Sigma-Aldrich). Next, 0.91 mmol of sodium oxalate ($Na_2C_2O_4$, purity $\geq$ 99.99%, Sigma-Aldrich) was added, and the mixture was stirred vigorously for 1 hour. The solution was then transferred to a Teflon-lined stainless-steel autoclave and heated at 473 K for 24 hours. The resulting product was rinsed three times with deionized water and ethanol using centrifugation (10 000 rpm, 15 minutes, RCF: 10 300 $\times$ *g*, rotor radius: 92 mm). It was subsequently dried at room temperature for 48 hours. The resulting product of this synthesis is Ni oxalate (NiC_2O_4) nanowires, which is the NiO precursor. NiO_{NW} is obtained after an annealing process at 773 K for 2 hours. A schema of the synthesis is shown in Fig. 1.

2.2. Characterization of NiO nanowires

Morphological and structural characterizations were performed on the synthesized NiO nanowires. Their morphology was examined through transmission electron microscopy (TEM) using an FEI Talos F200X microscope (Hillsboro, Oregon, US). The crystalline phases were identified using X-ray diffraction (XRD) with a Bruker D8 Advanced A25 DaVinci diffractometer (Billerica, Massachusetts, US), employing monochromatic Cu Kα radiation (8.04 keV), operated at 40 kV and 40 mA. The scanning range covered 2θ from 20° to 70° with a resolution of 0.02°. Structural characterization was performed using Raman spectroscopy with a HORIBA Scientific LabRAM HR Evolution Raman spectrometer. The instrument was equipped with a 532 nm DPSS laser excitation source, a X50 LD lens, and an 1800 lines per mm diffraction grating. Measurements were conducted in a backscattering configuration (emission and collection at the same angle) with an acquisition time of 10 s and a total of 10 accumulations. Finally, the chemical bonding and oxidation state of NiO were assessed *via* X-ray photoelectron spectroscopy (XPS) with a Kratos Analytical Ltd. Axis UltraDLD spectrometer (Manchester, UK) using monochromatic Al Kα radiation (1.49 keV) and a pass energy of 20 eV. The binding energy scale was accurate to within 0.1 eV, with electrostatic charging effects stabilized.

2.3. Nanofluid preparation

The NiO-based nanofluids analysed in this study were prepared using the synthesized NiO nanowires. The base fluid was a commercially available heat transfer fluid based on polydimethylsiloxane (PDMS), supplied by Wacker under the trade name Helisol 5A. This is a linear, non-reactive polydimethylsiloxane with a viscosity of approximately 5 $mm^2\ s^{-1}$. It is a clear, odourless and colourless liquid, featuring high heat resistance, a low pour point and non-corrosive properties. Three different

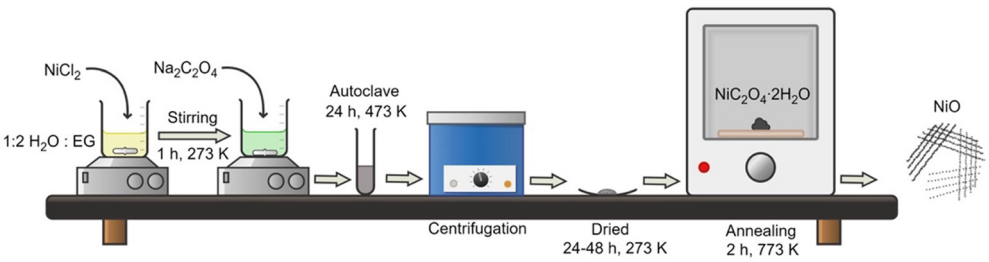

Fig. 1 Schema of the synthesis procedure used for obtaining NiO nanowires.

nanofluids were prepared using 100 mL of the base fluid and the necessary amount of synthesized NiO nanowires to achieve mass fractions of 0.01, 0.03, and 0.10 wt%. With these three-mass concentrations, nanofluids with and without surfactant were prepared to evaluate their influence on colloidal stability and thermal properties. SPAN20 (purity $\geq$ 44.0%, 1058 g cm^{-3} at 20 °C, Sigma-Aldrich) was used as the surfactant. A host fluid was prepared by mixing 0.01 wt% of SPAN20 and 100 mL of PDMS in an Elmasonic select 30 sonication bath at a frequency of 37 MHz for 10 minutes at 298 K. Next, the nanofluids were further processed using an Ultra-Turrax T18 supplied by IKA at 20 000 rpm with a 5 : 10 : 5 minute on:off:on cycle to prevent a significant temperature rise. Finally, the nanofluids were ready for colloidal stability characterization.

2.4. Nanofluid characterization

The stability of the prepared nanofluids was thoroughly analysed since this property is crucial in heat transfer applications. UV-Vis spectroscopy was employed to determine the extinction coefficient, which provides insight into the heat carriers in the fluid. The extinction coefficient values were measured using UV-Vis equipment assembled in our laboratory, featuring a DH-2000-BAL light source and a USB2000+ general-purpose spectrometer, both supplied by OceanOptics. Measurements of the extinction coefficient were taken at 500 nm, three times a day over a month. Additionally, particle size was measured using the dynamic light scattering (DLS) technique to assess the physical stability of the nanofluids. This technique allows the solvodynamic diameter of nanoparticles in suspension to be determined. The measurements were conducted using a Zetasizer Nano ZS instrument supplied by Malvern Instruments. Particle sizes were measured for over a month with three measurements taken daily.

The performance of nanofluids in heat transfer applications is influenced by several properties, including surface tension, density, dynamic viscosity, isobaric specific heat, and thermal conductivity. Consequently, these five properties were measured to characterize the nanofluids once they reached physical stability. These properties were then used to evaluate the application of nanofluids in CSP-PTC plants. Surface tension was measured using the pendant drop method with an OCA25 device supplied by DataPhysics. The dosage volume was set to 5 μL, with a dosage rate of 0.1 μL s^{-1}, using a Hamilton 250 μL syringe. Each nanofluid underwent ten measurements at 25 °C. Density was measured using the excitation pulse technique (DM densitometer, Anton Paar) at 25 °C, with five measurements performed for each nanofluid at room temperature. Dynamic viscosity was measured over a temperature range of 25 to 175 °C under steady-state conditions using a concentric cylinder geometry (bob diameter: 27.99 mm; bob length: 41.99 mm; cup diameter: 30.36 mm), with a shear rate ranging from 1 to 100 s^{-1}, using an HR10 rheometer supplied by TA Instruments.

Finally, thermal properties, specifically isobaric specific heat and thermal conductivity, were measured. Isobaric specific heat was determined using a temperature-modulated differential scanning calorimetry technique. The measurements were conducted using a DSC 214 Polyma calorimeter supplied by NETZSCH. The temperature program involved setting the temperature to 100 °C for 10 minutes to remove contaminants, followed by equilibration at 20 °C for 10 minutes, with a ramp rate of 10 °C min^{-1}. Subsequently, a temperature-modulated dynamic step from 20 to 205 °C was performed at 1 °C min^{-1}, with a modulation amplitude of ±1 °C and a period of 120 s to determine the isobaric specific heat. Finally, the cooling rate was set to 1 °C min^{-1}. Thermal conductivity was measured at various temperatures (from 25 to 100 °C) using the Transient Hot Bridge (THB) method, with a hot point sensor connected to a THB-100 system supplied by Linseis. To minimize natural convection during the measurements, a dry block heater (model DB 5.2) from IKA was used. This system was set between room temperature and 100 °C for thermal conductivity measurements, with an input power of 30 mW to ensure a good signal-to-noise ratio. Ten replicas were performed for each measurement, with a measurement time of 20 s and a 30 s delay between replicas to equilibrate the temperature.

3. Results and discussion

3.1. NiO nanowires characterization

The synthesis of NiO nanowires (NiO_{NW}) performed leads to an intermediate product being obtained, namely nickel(II) oxalate (NiC_2O_4), which is the precursor of NiO. XRD was used for the structural characterization of the nanoparticles under study to confirm the formation of the product of the synthesis. The crystallite sizes were also estimated. For comparison purposes, a commercial NiO (named as NiO_{com}) was analysed. Fig. 2(a) shows the diffraction patterns obtained for the NiC_2O_4 and NiO nanowire powders. XRD shows several diffraction peaks for NiC_2O_4 at 2θ values of 22.7°, 30.36°, 37.75° and 47.8°, which can be assigned to the diffraction of (002), (−402), (−204) and (−604) planes, aligning well with the reference data for the cubic phase of NiC_2O_4 (JCPDS no. 25-0851). This pattern clearly confirmed the formation of nickel oxalate. NiO nanowires were formed after the annealing process of NiC_2O_4. The pattern obtained for the nanowires is shown in Fig. 2(a), and it is clearly different to that obtained for NiC_2O_4 and similar to the pattern for commercial NiO. Thus, diffraction peaks for the synthesized nanowires and the commercial NiO were observed at 2θ of 37.1°, 43.1° and 62.7°, corresponding to the diffraction of the (111), (200), and (2 2 0) planes, respectively. These peaks match the reference data for the cubic phase of NiO (JCPDS no. 47-1049).[11] No evidence of other crystalline phases of NiO or foreign species was found in the patterns. Therefore, these results confirm the formation of NiO after the annealing process.

The average crystallite size of the NiO_{NW} was estimated to be 12.6 nm using the Debye–Scherrer equation,[12] with a shape factor of 0.94 and the full width at half maximum (FWHM) of the most intense peak, the (200) reflection. This result aligns well with the average diameter estimated from the TEM images,

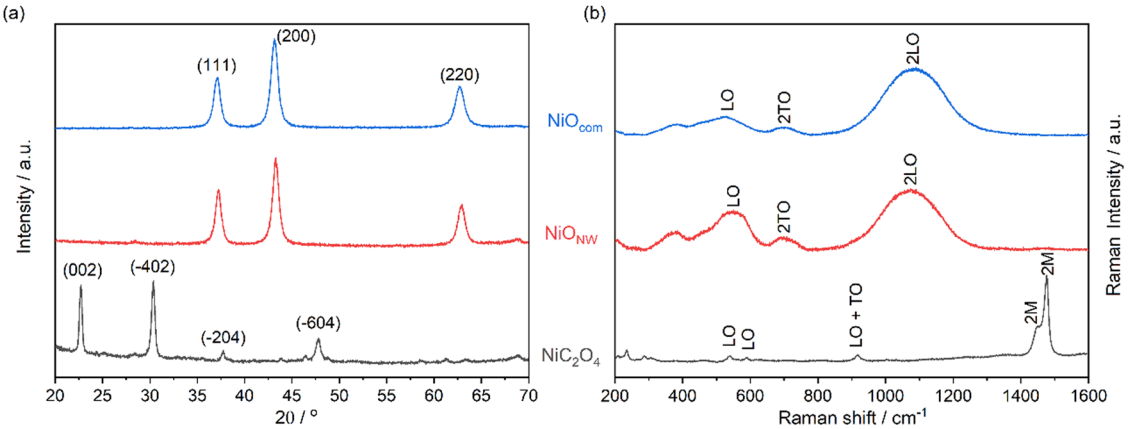

Fig. 2 (a) XRD patterns and (b) Raman spectra for NiC_2O_4, NiO_{NW} and NiO_{com}.

as is discussed below. The relative intensity of the peaks associated with the diffraction of the (111) and (200) planes indicate a predominant presence of these facets on the NiO grains, which is linked to the formation of thermodynamically favoured shapes. The particle size obtained for NiC_2O_4 was 24.6 nm.

Structural characterization was accomplished using Raman spectroscopy. Again, the Raman spectrum for commercial the NiO was recorded for comparison purposes. Fig. 2(b) further confirms the identity of the nickel(II) oxalate. It exhibits a series of low-intensity bands, two bands at 540 cm^{-1} and 590 cm^{-1}, corresponding to the longitudinal optical mode (LO) of a phonon, and a peak at 920 cm^{-1}, representing the combination of a longitudinal and an optical phonon (LO + TO). Additionally, a doublet is observed, comprising a high-intensity band at 1476 cm^{-1} and a low-intensity shoulder at 1448 cm^{-1}, which are attributed to the two-magnon band (2M) arising from the Ni^{2+}–O^{2-} vibration[13]. The analysis of the Raman spectra for the NiO nanowires and commercial NiO (Fig. 2(b)) showed the presence of three of the four characteristic NiO vibrational modes. Specifically, we observed a band centred between 530 and 540 cm^{-1}, which corresponds to the longitudinal optical mode, a band at 700 cm^{-1} attributed to two transverse optical phonons, and a band in the range of 1040–1080 cm^{-1}, representing two longitudinal phonons. The band expected at 925 cm^{-1}, which arises from the combination of a transverse and longitudinal phonon, was not detected. This is probably due to its overlap with and thus suppression by the intense 1040–1080 cm^{-1} band.[14] The Raman results confirmed the formation of NiC_2O_4 and NiO after annealing, as was shown previously by XRD.

XPS analysis was performed to investigate the chemical bonding and oxidation states of the NiO precursor, NiC_2O_4, the NiO nanowires and the commercial NiO, for comparison purposes. For all the analysed samples, the peak assignments were referenced to the adventitious C 1s signal at 284.8 eV. Fig. 3 presents the XPS spectra, including the Ni 2p (Fig. 3(a))

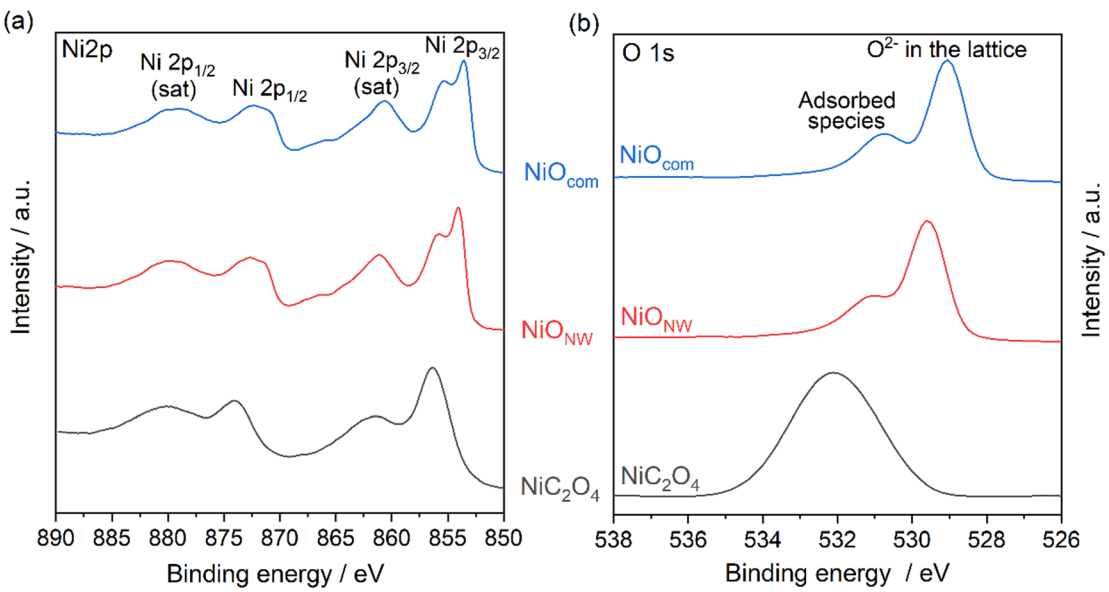

Fig. 3 (a) Ni 2p and (b) O 1s signals for NiC_2O_4, NiO_{NW} and NiO_{com}.

and O 1s (Fig. 3(b)) signals, for NiC_2O_4, NiO_{NW} and NiO_{com}. The Ni $2p_{1/2}$ signal NiC_2O_4 appears at a binding energy (BE) of 874.0 eV, while the contribution of Ni $2p_{3/2}$ is observed at a BE of 856.4 eV. This split spin–orbit component with a separation of 17.6 eV is typical for Ni(II) species.[15] Additionally, satellite peaks at BEs of about 880.2 and 861.4 eV are observed, and they are typical for the Ni signal. These binding energies align with the +2 oxidation state of Ni, suggesting the predominance of Ni(II) in the sample. The O 1s line of NiC_2O_4 exhibits the most intense peak at 532.6 eV, associated with oxalate ions ($C_2O_4^{2-}$). Specifically, this peak corresponds to the oxygen atoms within the O–C–O bonds.[16]

Furthermore, the Ni $2p_{3/2}$ and $2p_{1/2}$ contributions for both NiO_{NW} and NiO_{com} (Fig. 3(a)) appeared at BEs of about 854.2 and 871.9 eV, respectively, which are lower than for NiC_2O_4, as expected. Again, large spin–orbit splitting is observed, and satellites for both signals were found. But the most interesting feature is that the signal of Ni $2p_{3/2}$ for both NiO_{NW} and NiO_{com} exhibited a doublet, which is typical for Ni(II) in NiO.[17] On the other hand, the O 1s spectra (Fig. 3(b)) for both NiO_{NW} and NiO_{com} showed two contributions. The most intense contribution appears at about 529.0 eV, typical for the O^{2-} in the lattice. The other contribution appears at a BE of about 530.8 eV, and it corresponds to adsorbed species on the NiO surface.[18] Therefore, a good correlation was found between the commercial NiO and the nanowires synthesized. Thus, XPS results confirms the synthesis of NiO.

The morphology and nominal particle size of the NiO precursor, NiC_2O_4, and the synthesized NiO nanowires were studied using transmission electron microscopy (TEM). In addition, Fig. 4(a) shows representative images for NiC_2O_4, and the formation of nanowires can be observed. Size distribution analysis was conducted using lower magnification images. The average length was determined to be 2432 ± 143 nm, with lengths ranging from 1000 nm to 6000 nm, while the average thickness was found to be 60.5 ± 1.7 nm, with thicknesses ranging from 32 nm to 130 nm. Fig. 4(a) confirms the successful formation of NiO nanowires from the NiC_2O_4 precursor after the annealing process. As illustrated in Fig. 4(a), the nanowires exhibited a polycrystalline structure, consisting of sintered NiO grains with an average size of about 12.7 ± 0.2 nm, with a size range between 7 nm and 21 nm. This architecture is likely attributed to the formation of NiO crystals in thermodynamically favoured shapes such as octahedra, cuboctahedra, and cubes during the high-temperature calcination of nickel oxalate precursor at 773 K. The nominal length of the NiO nanowires was found to be non-uniform, ranging from 600 to 5500 nm. In contrast, the nominal diameter was relatively consistent across all observed nanowires, averaging approximately 45 ± 1.5 nm. Finally, the successful formation of NiO nanowire was further supported by annular dark-field images (Fig. 4(b)) and the elemental EDX analysis performed. Fig. 4(b) shows the homogeneous distribution of Ni and O in the nanowires.

3.2. Nanofluid stability

The colloidal stability of the NiO_{NW} nanofluids, both with and without surfactant, was investigated. The samples without surfactant were dispersed in PDMS and those with were prepared using a 0.1 wt% SPAN20 solution in PDMS, which acts as host fluid. Since nanofluids are susceptible to particle aggregation and sedimentation, stability was assessed through extinction coefficient and particle size analysis, as described above. UV-Vis spectra were used to determine extinction coefficients, which quantify light absorption and scattering, and thus provide information on heat carrier concentration. Fig. 5 displays the extinction coefficient values at 500 nm for the NiO_{NW} nanofluids, recorded over 30 days. Immediately after the preparation of the nanofluids, higher NiO concentrations correlate with higher extinction coefficient values, as expected. All the nanofluids exhibited aggregation during the first few days post-preparation,

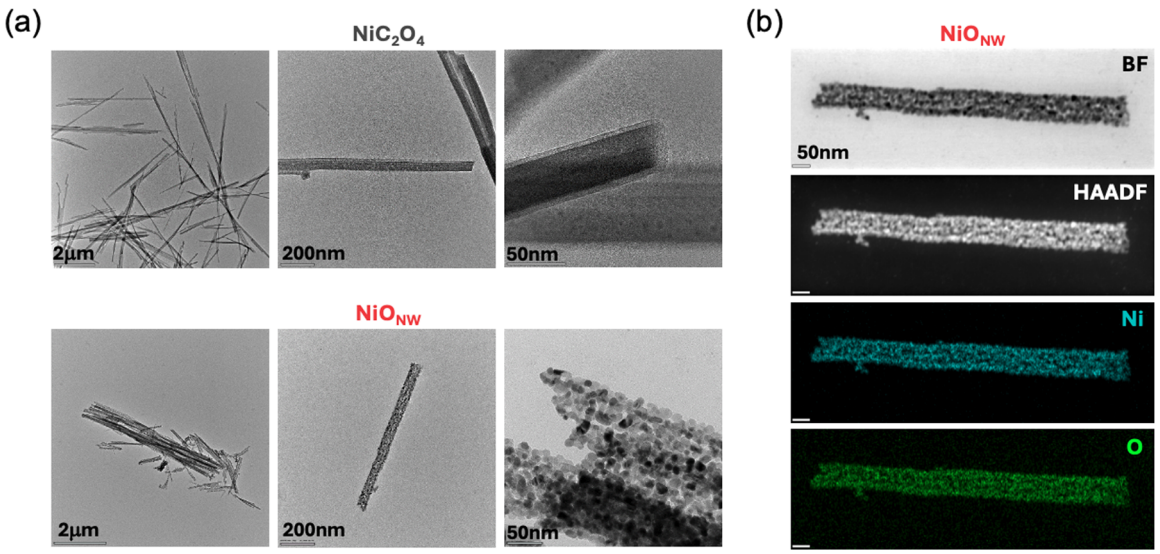

Fig. 4 (a) TEM images for NiC_2O_4 and NiO_{NW}. (b) Annular dark-field images and EDX elemental maps for NiO_{NW}.

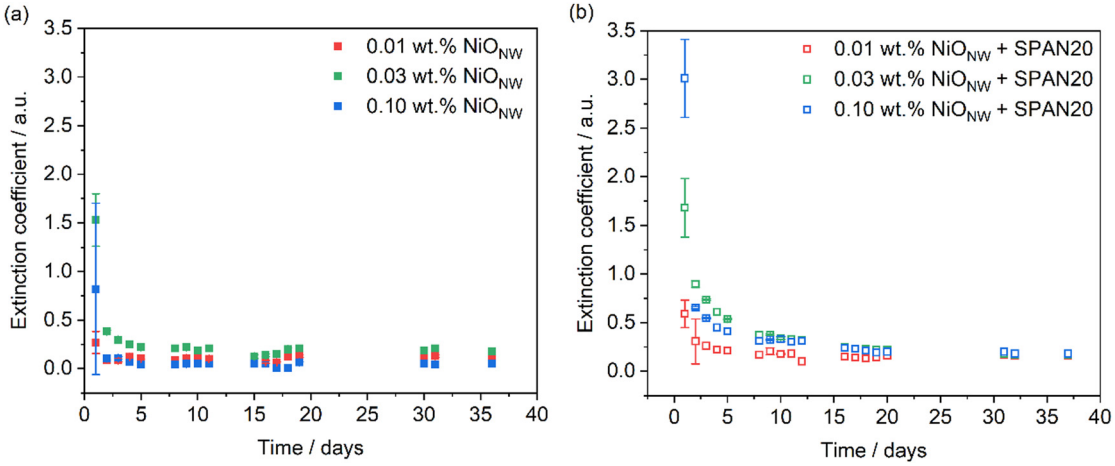

Fig. 5 Extinction coefficient values for nanofluids prepared using (a) NiO_{NW} without surfactant, and (b) NiO_{NW} with surfactant, obtained by UV-Vis spectroscopy at λ = 500 nm.

evidenced by a decline in extinction coefficient values. Subsequently, these values stabilized with minimal fluctuations, indicating equilibrium being reached. Moreover, in all the cases, when the nanofluids reached stability, the extinction coefficient values were similar in every case. The sedimentation process was faster for the nanofluids without surfactant (Fig. 5(a)). In the case of the nanofluids with surfactant (Fig. 5(b)), the sedimentation process was slower, stability reached after about 7 days.

Fig. 6 shows the particle size distribution of the NiO_{NW} nanofluids, prepared without surfactant (Fig. 6(a)) and with surfactant (Fig. 6(b)). In the case of the nanofluid with the lowest NiO concentration and without SPAN20 (Fig. 6(a)), the particle size values initially increased during the aggregation period, followed by a dramatic decrease within 10 days. This is attributed to the low concentration of NiO nanoparticles in suspension, as previously inferred from the extinction coefficient values. The results for this nanofluid also showed low goodness and high deviation due to the low concentration of nanowires in suspension; therefore, the characterization was stopped after 12 days. The other two nanofluids prepared with surfactant and a higher nominal concentration exhibited a similar initial increase in particle size during aggregation, followed by a decrease to several hundred nanometres. These values then remained relatively constant, indicating stability being reached. However, a significant deviation in the values was observed for all the nanofluids during the initial hours. This is due to nanofluids being a dynamic system, the formation of aggregates changing. The nanofluids prepared without surfactant exhibited a higher deviation of the particle size over a longer time, suggesting heightened instability within these systems (Fig. 6(a)). However, but at the end of the characterization period, the nanofluids seemed to reach a certain stability. These results corroborate the findings obtained from the extinction coefficient measurements.

Finally, the extinction coefficient and particle size values were observed to reach a plateau over time in the nanofluids with the surfactant, suggesting that they reached a certain stability. The incorporation of the surfactant seems to allow a more controlled system, with changes slower, but the surfactant does not result in more nanowires in suspension. This behaviour

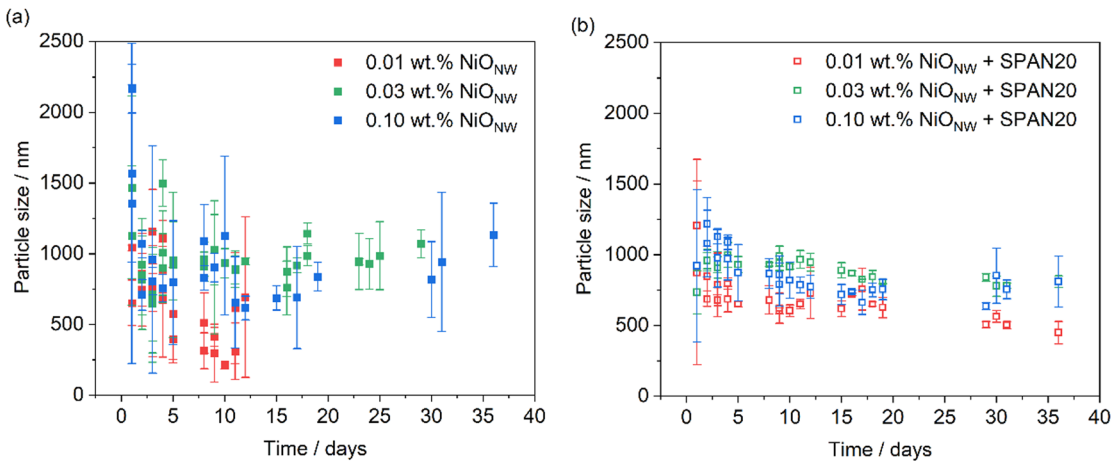

Fig. 6 Particle size distributions for nanofluids prepared using (a) NiO_{NW} without surfactant, and (b) NiO_{NW} with surfactant, obtained by DLS.

can be attributed to the inherent properties of the base fluid; its low surface energy hinders its reactivity and restricts interactions with metal oxide nanoparticles[19]. Therefore, the nanofluids reached a certain level of stability but with a low concentration of heat carriers.

3.3. Nanofluid properties

The heat transfer coefficient (h) of a heat transfer fluid, directly related to the Mouromtseff number (Mo), is a crucial parameter for assessing thermal performance and efficiency. Since Mo is influenced by fluid properties such as density, surface tension, viscosity, specific heat, and thermal conductivity, these properties were measured for the nanofluids to evaluate their suitability for heat transfer applications.

3.3.1. Surface tension. Surface tension values are shown in Table 1. They exhibited minimal variation for all the nanofluids, with a slight decrease observed compared to the PDMS used as the base fluid. As expected, the addition of the surfactant, SPAN20, led to a reduction in surface tension. However, it is important to note that changes in surface tension typically have a negligible impact on heat transfer within single-phase systems. In contrast, density and dynamic viscosity significantly influence flow patterns, consequently affecting convective heat transfer and pressure losses within the system.

3.3.2. Density. Density is a fundamental property in heat transfer phenomena. Extensive research has demonstrated that the incorporation of nanoparticles into base fluids results in an increased density of the nanofluid, attributable to the higher intrinsic density of the nanoparticles.[20] The density of the base fluid at 298 K was measured at 918.14 ± 0.05 kg m^{-3}, which is in excellent agreement with the value supplied by the manufacturer, that is 918.8 kg m^{-3} at the same temperature.[21] The density values obtained for all the nanofluids are summarized in Table 1. These values were slightly higher than that of the base fluid, as expected given the higher density of the nanoparticles, 0.057% being the biggest increase, which is within the uncertainty of the measurements. Regarding the concentration, no significant density differences were observed for the nanofluids with varying amounts of nanowires, which is in good agreement with the extinction coefficient values shown previously. These results suggest that the inert nature of the base fluid only allows a limiting value of nanoparticles in suspension, indicating that the system may reach a saturation point for nanoparticle loading.

Table 1 Values of density, ρ, the increase in density with respect to the pure PDMS, $\Delta\rho$, and surface tension, γ, for the nanofluids and the base fluids

HTF	γ/mN m^{-1}	ρ/kg m^{-3}	$\Delta\rho$/%
Base Fluid	18.76 ± 0.01	918.14 ± 0.05	—
Host fluid (PDMS + SPAN20)	18.73 ± 0.01	917.90 ± 0.00	—
0.01 wt% NiO_{NW}	18.74 ± 0.01	918.34 ± 0.05	0.022
0.03 wt% NiO_{NW}	18.69 ± 0.01	918.44 ± 0.05	0.033
0.10 wt% NiO_{NW}	18.72 ± 0.01	918.54 ± 0.05	0.044
0.01 wt% NiO_{NW} + SPAN20	18.71 ± 0.01	918.50 ± 0.07	0.039
0.03 wt% NiO_{NW} + SPAN20	18.70 ± 0.01	918.66 ± 0.05	0.057
0.10 wt% NiO_{NW} + SPAN20	18.70 ± 0.01	918.52 ± 0.04	0.041

3.3.3. Dynamic viscosity. Typically, adding nanoparticles to a fluid increases its viscosity, a disadvantage in heat transfer applications due to higher pumping energy and pressure drops.[22] Therefore, the rheological behaviour and the dynamic viscosity values were measured to analyse the effect of the suspension of NiO nanostructures in the PDMS.

In order to analyse the rheological behaviour, the shear flow plots were recorded using a concentric cylindrical geometry in the 298–448 K temperature range. Fig. 7 shows the plots for the PDMS and for the solution of SPAN20 in PDMS (Fig. 7(a)), in addition to the nanofluids prepared using NiO nanowires without surfactant (Fig. 7(b)) and with surfactant (Fig. 7(c)). The nanofluids presented a similar behaviour to the base fluid. All fluids exhibited Newtonian behaviour characterized by constant apparent viscosity within a shear rate range of about 5–40 s^{-1}. The observation of the Newtonian behaviour in a small shear rage range is a known limitation of the measurement geometry used.[23]

Dynamic viscosity values were extracted from these plots in the shear rate range described above, the values obtained shown in Fig. 8. The viscosity of the base fluid was found to be 5.29 mPa s at 298 K, closely matching the value of 5.34 mPa s given by the supplier,[24] a deviation of about 1%. The base fluid and NiO-based nanofluids exhibited a decrease in viscosity as the temperature increased, as expected. The dynamic viscosity values for the nanofluids did not increase significantly compared to those of the base fluid, which is a similar behaviour for other nanofluids prepared using the PDMS as the base fluid.[23] In some cases, a slight decrease in viscosity was observed, but these differences are within the experimental uncertainty.[25] In addition, the dynamic viscosity values of the nanofluids did not change significantly, either with increasing the nanoparticle concentration or in the presence of SPAN20. This can be attributed to the limited quantity of nanowires in suspension, as discussed in the stability section, indicating that colloidal stability has a maximum particle concentration which remained quasi unchanged in all cases. In summary, all the NiO-based nanofluids presented only a negligible increase in dynamic viscosity compared to the base fluid, which is a good result for the application of our nanofluids in heat transfer processes.

3.3.4. Isobaric specific heat. For nanofluids, especially in heat transfer applications, isobaric specific heat is a critical property that defines their heat storage capacity. This study measured the isobaric specific heat of all the NiO-based nanofluids and the base fluid, as shown in Fig. 9. The specific heat capacity of the base fluid, measured at 298 K, was determined to be 1.544 J g^{-1} K^{-1}. This value showed a relative deviation of 2.1% compared to the value given by the supplier, that is 1.587 J g^{-1} K^{-1} at the same temperature,[24] indicating satisfactory measurement accuracy. The relative standard deviation of the experimental measurements was less than 1.0%. The most interesting result is the difference between the behaviour of the nanofluids prepared with (Fig. 9(b)) or without surfactant

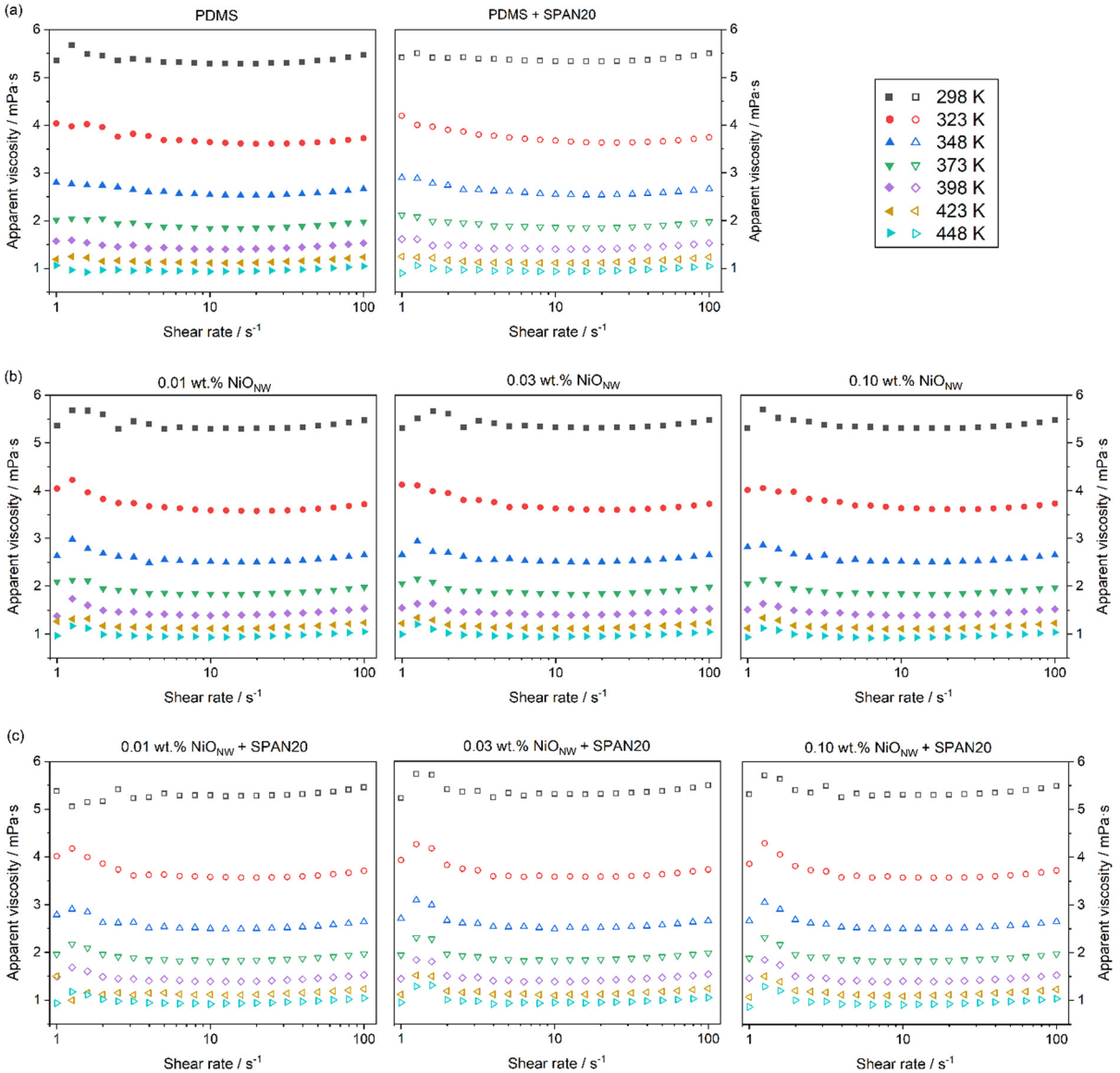

Fig. 7 Shear stress flow plots for: (a) the PDMS, and the solution of SPAN20 in PDMS, (b) the nanofluids without surfactant, and (c) with surfactant, at temperatures from 298 K to 448 K.

(Fig. 9(a)). The nanofluids prepared with surfactant show similar values compared to the pure PDMS, while those without show a slight increase in isobaric specific values, as shown in Fig. 9(a). The increase is up to 4%, the nanofluid prepared with the highest nominal concentration showing the highest values. The differences between the three nanofluids are slight, however, within the uncertainty of the measurements. Despite the increase being slight, these isobaric specific heat values for the nanofluids without surfactant are interesting due to the small amount of NiO that the base fluid supports, as shown by the extinction coefficient of the nanofluids (Fig. 6). These values are in line with previous studies that have reported increases in isobaric specific heat for various nanofluids,[26] and elucidating the underlying mechanisms of this molecular configuration of the fluid phenomenon is of significant interest. Typically, it is attributed to the surrounding the nanomaterial and the strength of the interactions between the system components.[26b,c]

3.3.5. Thermal conductivity. Thermal conductivity is a critical property for assessing heat transfer fluid performance. This property was measured for all the NiO_{NW}-based nanofluids, and the base fluid for comparison purposes. The measured thermal conductivity for the base fluid at 25 °C was 0.1251 W m^{-1} K^{-1}, closely aligning with the supplier's reported value of 0.126 W m^{-1} K^{-1},[24] demonstrating a 0.7% deviation. Fig. 10 shows the thermal conductivity values for all the NiO-based nanofluids and the base fluid across the temperature range of 298–384 K. All the nanofluids, once stabilized, exhibited a low concentration of suspended nanowires, as shown in Fig. 5. However, the results suggest an increase in thermal

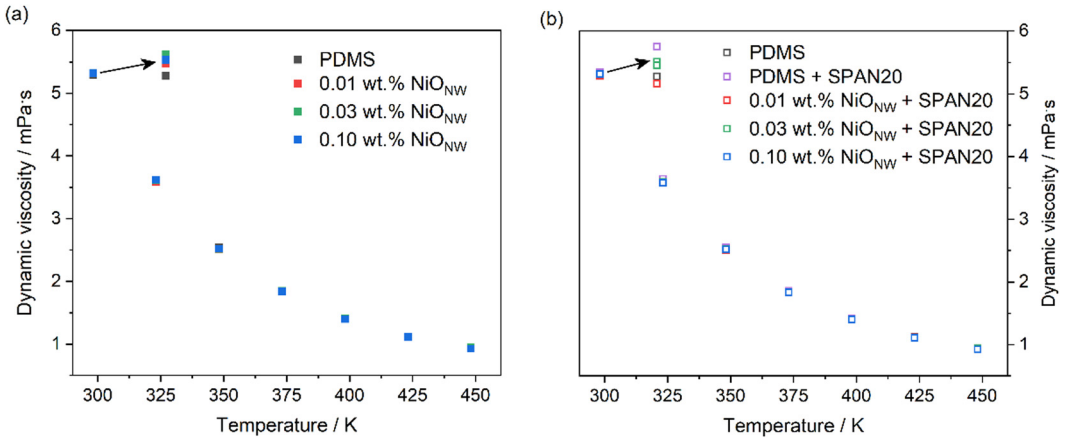

Fig. 8 Dynamic viscosity values for nanofluids prepared using (a) NiO_{NW} without surfactant, and (b) NiO_{NW} with surfactant, in the 298–448 K temperature range.

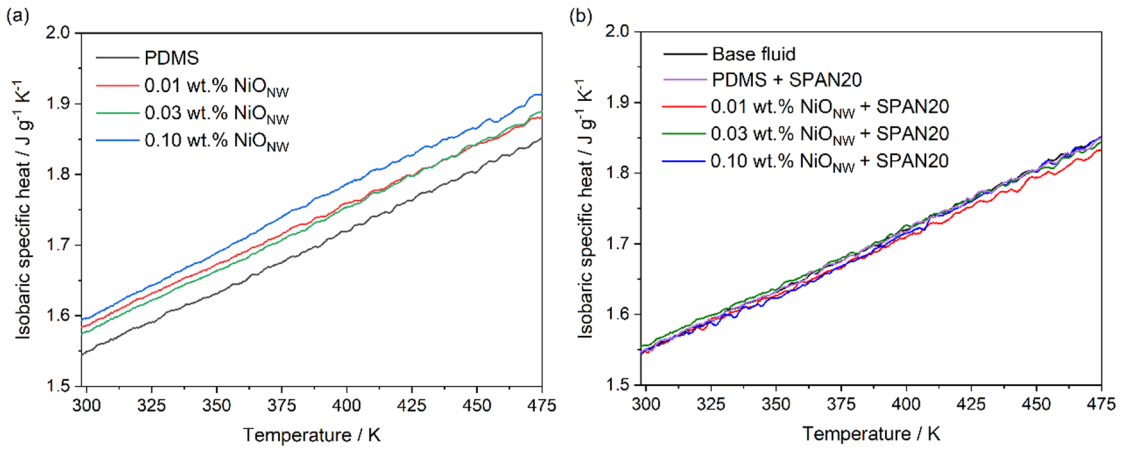

Fig. 9 Isobaric specific heat values for nanofluids prepared using (a) NiO_{NW} without surfactant, and (b) with surfactant, in the 298–475 K temperature range.

conductivity for the nanofluids relative to the base fluid of up to 3% (Fig. 10), which is similar to nanofluids based on oxides, for example CuO, reported in the literature.[26d] Nevertheless, all the measured thermal conductivity values were within the uncertainty of the method.

3.4. Nanofluid performance in CSP-PTC

The performance in a CSP-PTC system of the nanofluids prepared in this work has been evaluated by using a phenomenological model that allows the efficiency to be estimated of the parabolic trough collector and the heat exchanger typically designed for this application. The collector efficiency (ψ_{coll}) was evaluated using the analytics expressions reported previously in the literature by Bellos *et al.*[27] and O'Keeffe.[28] The initial conditions considered are that the flow is under turbulent flow and steady-state conditions. In turn, the heat exchanger efficiency (ψ_{hex}) was estimated using the number of transfer units (NTU) methodology. The total efficiency of the system (ψ_{sys}) was calculated as $\psi_{sys} = \psi_{coll} \cdot \psi_{hex}$. These efficiencies were estimated for the pure PDMS because it is a fluid used in CSP-PTC plants, and for one of the nanofluids prepared. The nanofluid chosen was the one prepared without surfactant because all its properties were similar to those of the nanofluids with surfactant, except the isobaric specific heat, which was higher for the nanofluids prepared without surfactant. The lowest concentration of NiO nanowires was chosen because the properties measured did not increase significantly with the concentration, and using a low concentration to prepare the nanofluids costs less. All the details of the equations, variables and parameters used are described in greater depth in the (ESI†). Fig. 11 shows the values obtained for the efficiency of the collector, the heat exchanger and the overall system for several flow rate values, between 100 and 300 L min^{-1}. The collector efficiency values do not change significantly for the nanofluids with respect to the pure PDMS (Fig. 11(a)), probably due to the non-significant changes in the thermal properties. However, the heat exchanger is more efficient when the nanofluid is used, as shown in Fig. 11(b). An enhancement of about 4.5% was observed for all the flow rates tested. This enhancement in the heat exchanger

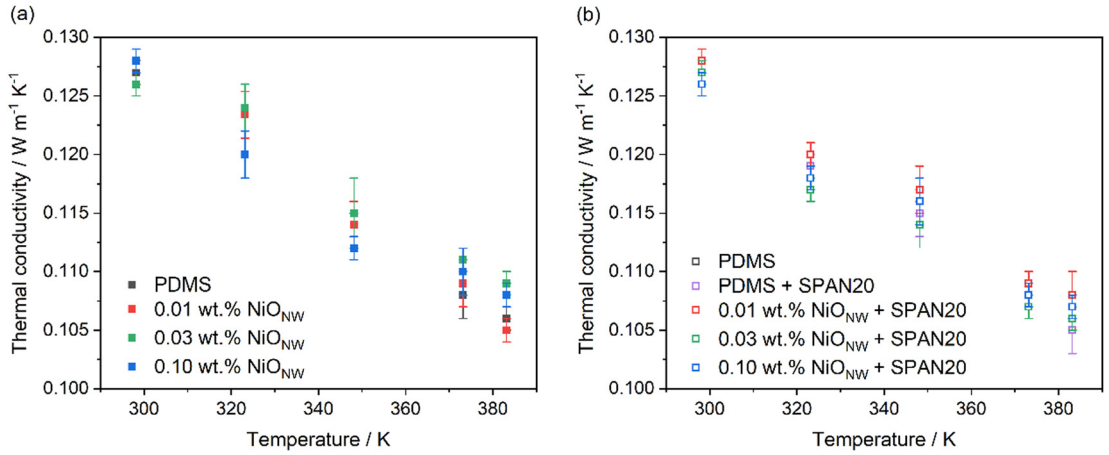

Fig. 10 Thermal conductivity values for nanofluids prepared using (a) NiO_{NW} without surfactant, and (b) with surfactant, in the 298–384 K temperature range.

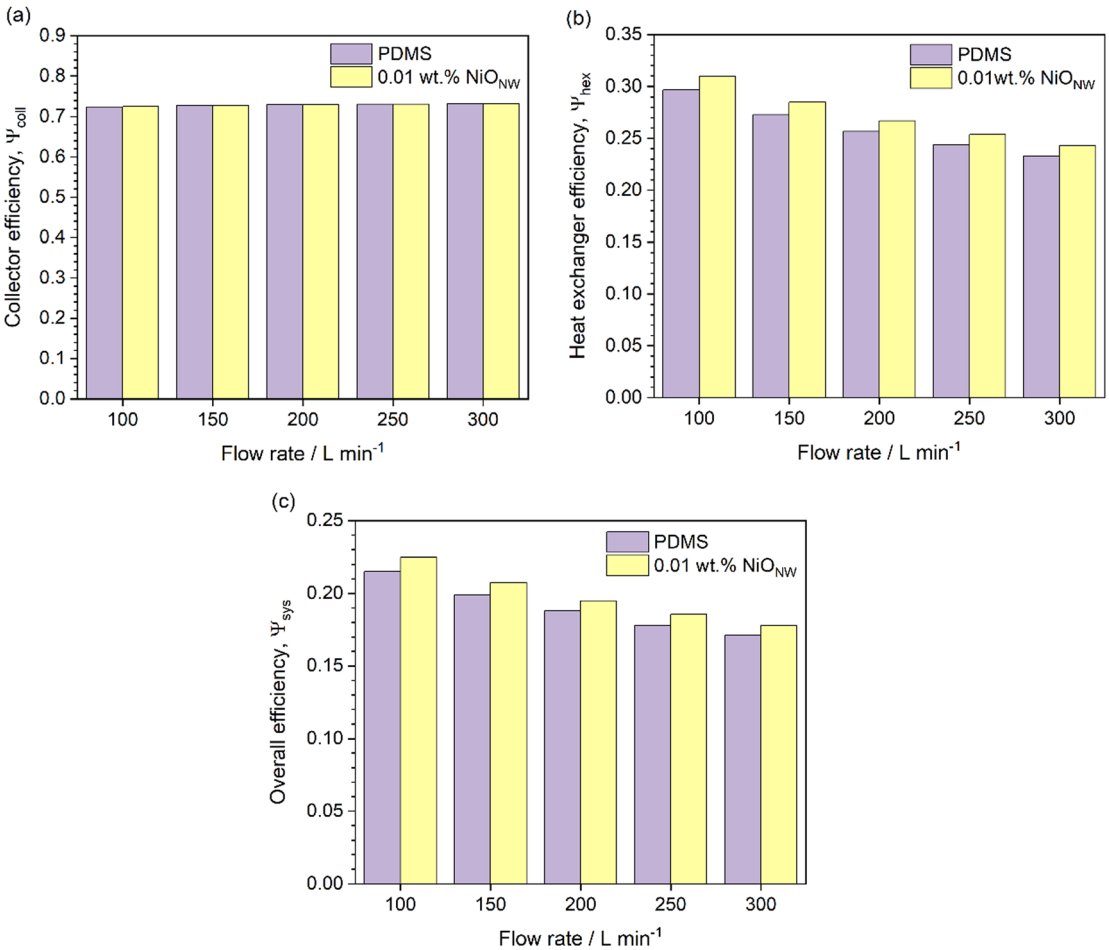

Fig. 11 (a) Efficiencies of (a) the PTC collector, (b) the heat exchanger and (c) the overall CSP-PTC system.

efficiency leads to an increase in the overall efficiency of the CSP-PTC system, as observed in Fig. 11(c). The estimated increase is about 5% when nanofluid is tested. This increase is not very high, but we have to bear in mind that a low concentration of nanowires is kept in suspension. Therefore, efforts to improve the suspension of this kind of material in the PDMS used are needed to enhance the performance of the nanofluids.

4. Conclusions

Nanofluids based on NiO nanowires and a polydimethylsiloxane (PDMS) fluid were developed to improve the efficiency of parabolic trough-based concentrating solar power plants (CSP-PTC). To this end, NiO nanowires were successfully synthesized in our laboratory and used to prepare nanofluids with and without surfactant. Their physical stability was thoroughly characterized. In both cases, the nanofluids reached a certain stability but with a low concentration of nanowires in suspension. Subsequently, the properties of interest for heat transfer applications were characterized. The changes in surface tension, density and dynamic viscosity were non-significant with respect to the pure PDMS used as the base fluid. In addition, isobaric specific heat increased by 4% in the case of the nanofluids prepared without surfactant. Moreover, the thermal conductivity of all the nanofluids increased by up to 3%.

Finally, a theoretical analysis was performed of the effect of the use of nanofluids in CSP-PTC system. The efficiencies of the collector and the heat exchanger were estimated to obtain the overall efficiency of CSP-PTC plants. The collector efficiency did not improve by using nanofluids, but the heat exchanger efficiency improved by 4.5%, leading to an increase in the overall efficiency of the CSP-PTC system of about 5%. This increase is not very high, but we must bear in mind that a low concentration of nanowires is kept in suspension. Therefore, efforts to improve the suspension of this kind of material in the PDMS used are needed to enhance the performance of the nanofluids.

Author contributions

D. D. S.: investigation, methodology, writing – original draft; J. J. G.: investigation, methodology; I. C.-B.: investigation, methodology, visualization, writing – original draft; M. G.-G.: investigation, methodology; S. G.-G.: investigation, methodology; V. G.: investigation; R. A.: investigation, methodology; J. N.: funding acquisition, project administration, supervision, writing – review and editing.

Conflicts of interest

There are no conflicts to declare.

Data availability

All relevant data are within the manuscript and the ESI.†

Acknowledgements

This work was supported by Ministerio de Ciencia, Innovación y Universidades, Agencia Estatal de Investigación, MICIU/AEI/10.13039/501100011033, and ERDF/EU [grant number PID 2023-150345OB-I00]; also to MCIN/AEI/10.13039/501100011033 and European Union "NextGenerationEU"/PRTR" [grant number TED2021-132518B-I00]. María Gragera-García acknowledges support under fellowship no. FPU23/01837, funded by MICIU/AEI/10.13039/501100011033, Ministerio de Ciencia, Innovación y Universidades, Agencia Estatal de Investigación, del Gobierno de España.

References

1 D. Dewanjee and B. Kundu, A review of applications of green nanofluids for performance improvement of solar collectors, *Renewable Energy*, 2025, **240**, 122182; S. Kulandaivel, N. W. Keng, M. Samykano, S. K. Suraparaju, M. F. Ghazali, R. K. Rajamony and N. S. A. Ghafar, MXene nanofluids in advanced applications: An in-depth review of thermophysical characteristics and technological innovations, *Mater. Today Sustain.*, 2025, **29**, 101084; S. A. Kadhim, K. A. Hammoodi, A. H. Askar, F. L. Rashid and H. A. A. Wahhab, Feasibility review of using copper oxide nanofluid to improve heat transfer in the double-tube heat exchanger, *Results Eng.*, 2024, **24**, 103227; U. S. Behera, J. S. Sangwai and H. S. Byun, A comprehensive review on the recent advances in applications of nanofluids for effective utilization of renewable energy, *Renewable Sustainable Energy Rev.*, 2025, **207**, 114901.

2 C. Hilgert, C. Jung, C. Wasserfuhr, J. Leon and L. Valenzuela, Qualification of silicone based HTF for parabolic trough collector applications, *AIP Conf. Proc.*, 2019, **2126**, 080003.

3 (*a*) F. Boufoudi, S. Zouaoui and S. Mihoub, Investigation of the Thermophysical Properties of Nanofluids Based on Metal Oxides: Application in Concentrated Solar Power Plants, *J. Technol. Innov. Energy*, 2023, **2**, 56; (*b*) G. F. Smaisim, W. A. AbdulHussein and A. M. Abed, Enhancement of heat transfer from solar thermal collector using nanofluid, *Open Eng.*, 2022, **12**, 968.

4 A. P. Nagvenkar, I. Perelshtein and A. Gedanken, *J. Phys. Chem. C*, 2017, **121**, 26551.

5 D. M. De Los Santos, I. Carrillo-Berdugo, A. Domínguez-Núñez, J. Antonio Poce-Fatou, D. Zorrilla and J. Navas, NiO nanowire-containing heat transfer nanofluids for CSP plants: Experiments and simulations to promote their application, *J. Mol. Liq.*, 2022, **360**, 119593.

6 I. Carrillo-Berdugo, J. Sampalo-Guzmán, A. Domínguez-Núñez, T. Aguilar, P. Martínez-Merino and J. Navas, Are Nanofluids Suitable for Volumetric Absorption in PTC-CSP Plants? An Exemplified, Realistic Assessment with Characterized Metal−Oil Nanofluids, *Energy Fuels*, 2022, **36**, 8413.

7 P. Padmaja and H. Soni, Nanofluids: Preparation Methods and Challenges in Stability, *Nanofluids and Their Engineering Applications*, CRC Press, Boca Raton, USA, 2019, p. 1; Y. Chen, X. Quan, Z. Wang, C. Lee, Z. Wang, P. Tao, C. Song, J. Wu, W. Shang and T. Deng, Stably dispersed high-temperature Fe_3O_4/silicone-oil nanofluids for direct solar thermal energy harvesting, *J. Mater. Chem. A*, 2016, **4**, 17503.

8 M. A. B. Harun, N. A. C. Sidik and M. A. M. Rohaizan, Experimental investigation of stability and thermal

properties of nanocellulose-water nanofluid, *IOP Conf. Ser.: Mater. Sci. Eng.*, 2020, **1092**, 012044.
9 K. A. Jehhef and M. A. A. A. Siba, Effect of surfactant addition on the nanofluids properties: A review, *Acta Mech. Malays.*, 2019, **2**, 1.
10 T. T. L. Dang and M. Tonezzer, Polycrystalline NiO Nanowires: Scalable Growth and Ethanol Sensing, *Procedia Eng.*, 2015, **120**, 427.
11 D. Wu, L. Zhang, J. Zhang, Z. Zhang, F. Liang, L. Jiang, B. Tang, Y. Rui and F. Liu, Novel self-supporting multilevel-3D porous NiO nanowires with metal-organic gel coating via ''like dissolves like'' to trigger high-performance binder-free lithium-ion batteries, *Microporous Mesoporous Mater.*, 2021, **328**, 111483.
12 R. Bajaj, A. S. Rao and G. V. Prakash, Linear and nonlinear photoluminescence from thermally stable KYF4:Eu^{3+} cubic nanocrystals, *J. Alloys Compd.*, 2021, **885**, 160893.
13 K. K. Sahu, R. K. Sahoo, L. D. Beshra and M. Mohapatra, Facile synthesis of nickel oxalate@ carbon as electrical double layer and its derived nickel oxide as pseudo-type supercapacitor electrodes, *Ionics*, 2021, **27**, 819.
14 C. Liu, C. Li, K. Ahmed, Z. Mutlu, C. S. Ozkan and M. Ozkan, Template Free and Binderless NiO Nanowire Foam for Li-ion Battery Anodes with Long Cycle Life and Ultrahigh Rate Capability, *Sci. Rep.*, 2016, **6**, 29183.
15 T. Montoya, A. Amrollahi, G. Vitale, N. Hosseinpour and N. N. Nassar, Size Effects of NiO Nanoparticles on the Competitive Adsorption of Quinolin-65 and Violanthrone-79: Implications for Oil Upgrading and Recovery, *ACS Appl. Nano Mater.*, 2020, **3**, 5311.
16 S. P. Chenakin and N. Kruse, XPS characterization of transition metal oxalates, *Appl. Surf. Sci.*, 2020, **515**, 146041.
17 P. S. Bagus, C. J. Nelin, C. R. Brundle, B. V. Crist, E. S. Ilton, N. Lahiri and K. M. Rosso, Gold–Aluminyl and Gold–Diarylboryl Complexes: Bonding and Reactivity with Carbon Dioxide, *Inorg. Chem.*, 2022, **61**, 18077.
18 K. Chandra Sekhar Reddy, P. Sahatiya, I. Santos-Sauceda, O. Cortázar and R. Ramírez-Bon, One-step fabrication of 1D p-NiO nanowire/n-Si heterojunction: Development of self-powered ultraviolet photodetector, *Appl. Surf. Sci.*, 2020, **513**, 145804.
19 O. T. Mefford, M. L. Vadala, J. D. Goff, M. R. J. Carroll, R. Mejia-Ariza, B. L. Caba, T. G. St. Pierre, R. C. Woodward, R. M. Davis and J. S. Riffle, Stability of polydimethylsiloxane-magnetite nanoparticle dispersions against flocculation: interparticle interactions of polydisperse materials, *Langmuir*, 2008, **24**, 5060.
20 Z. Said, M. A. Abdelkareem, H. Rezk and A. M. Nassef, Fuzzy modeling and optimization for experimental thermophysical properties of water and ethylene glycol mixture for Al_2O_3 and TiO_2 based nanofluids, *Powder Technol.*, 2019, **353**, 345.
21 B. Mehta, D. Subhedar, H. Panchal and Z. Said, Synthesis, stability, thermophysical properties and heat transfer applications of nanofluid – A review, *J. Mol. Liq.*, 2022, **364**, 120034.
22 T.-H. Tsai, L.-S. Kuo, P.-H. Chen and C.-T. Yang, Effect of viscosity of base fluid on thermal conductivity of nanofluids, *Appl. Phys. Lett.*, 2008, **93**, 233121.
23 D. De los Santos, J. J. Gallardo, I. Carrillo-Berdugo, R. Alcántara and J. Navas, Efficient nanofluids based on Ag nanoparticles and a linear silicone-based fluid for concentrating solar power, *J. Mol. Liq.*, 2024, **413**, 125898.
24 **https://www.wacker.com/h/en-us/medias/HELISOL-5A-en-2024.06.16.pdf**.
25 P. Martínez-Merino, S. D. Midgley, E. I. Martín, P. Estellé, R. Alcántara, A. Sánchez-Coronilla, R. Grau-Crespo and J. Navas, Novel WS2-Based Nanofluids for Concentrating Solar Power: Performance Characterization and Molecular-Level Insights, *ACS Appl. Mater. Interfaces*, 2020, **12**, 5793.
26 (*a*) D. De los Santos, J. J. Gallardo, I. Carrillo-Berdugo, R. Alcántara, P. Estellé, S. Gragera, M. Gragera and J. Navas, Nanofluids Based on Pd Nanoparticles and a Linear Silicone-Based Fluid: Toward Highly Efficient Heat Transfer Fluids for Concentrated Solar Power, *ACS Sustainable Chem. Eng.*, 2024, **12**, 2375; (*b*) I. Carrillo-Berdugo, S. D. Midgley, R. Grau-Crespo, D. Zorrilla and J. Navas, Understanding the Specific Heat Enhancement in Metal-Containing Nanofluids for Thermal Energy Storage: Experimental and *Ab Initio* Evidence for a Strong Interfacial Layering Effect, *ACS Appl. Energy Mater.*, 2020, **3**, 9246; (*c*) I. Carrillo-Berdugo, R. Grau-Crespo, D. Zorrilla and J. Navas, Interfacial molecular layering enhances specific heat of nanofluids: Evidence from molecular dynamics, *J. Mol. Liq.*, 2021, **325**, 115217; (*d*) J. J. Gallardo, S. Gragera, M. Gragera, I. Carrillo-Berdugo, D. De los Santos, R. Alcántara and J. Navas, Nanofluids for concentrating solar power based on CuO nanoparticles and a linear silicone fluid, *Sol. RRL*, 2025, e2500089.
27 E. Bellos and C. Tzivanidis, Analytical Expression of Parabolic Trough Solar Collector Performance, *Designs*, 2018, **2**, 9.
28 G. J. O'Keeffe, S. L. Mitchell, T. G. Myers and V. Cregan, Modelling the efficiency of a nanofluid-based direct absorption parabolic trough solar collector, *Sol. Energy*, 2018, **159**, 44.